

NCI PLOT and the analysis of noncovalent interactions using the reduced density gradient

Rubén Laplaza^{1,2} | Francesca Peccati^{1,3} | Roberto A. Boto^{1,4} | Chaoyu Quan^{3,5} |
 Alessandra Carbone^{6,7} | Jean-Philip Piquemal^{1,7} | Yvon Maday^{5,7} |
 Julia Contreras-García¹ 

¹CNRS, Laboratoire de Chimie Théorique, LCT, Sorbonne Université, Paris, France

²Departamento de Química Física, Universidad de Zaragoza, Zaragoza, Spain

³Institut des Sciences du Calcul et des Données, ISCD, Sorbonne Université, Paris, France

⁴Centro de Física de Materiales CFM-MPC (CSIC-UPV/EHU), Donostia, Spain

⁵SUSTech International Center for Mathematics, and Department of Mathematics, Southern University of Science and Technology, Shenzhen, China

⁶CNRS, IBPS, Laboratoire de Biologie Computationnelle et Quantitative (LCQB), Sorbonne Université, Paris, France

⁷Institut Universitaire de France, Paris, France

Correspondence

Julia Contreras-García, Sorbonne Université, CNRS, Laboratoire de Chimie Théorique, LCT, Paris 75005, France.
 Email: contrera@lct.jussieu.fr

Funding information

Agence Nationale de la Recherche, Grant/Award Numbers: ANR-11-IDEX-0004-02, ANR-11-LABX-0037-01; PICS-CNRS; Ecole doctorale 388; H2020 European Research Council, Grant/Award Number: 810367; Institut Universitaire de France; PHC PROCOPE 2017

Abstract

Noncovalent interactions are of utmost importance. However, their accurate treatment is still difficult. This is partially induced by the coexistence of many types of interactions and physical phenomena, which hampers generality in simple treatments. The NCI index has been successfully used for nearly over 10 years in order to identify, analyze, and understand noncovalent interactions in a wide variety of systems, ranging from proteins to molecular crystals. In this work, the development and implications of the method will be reviewed, and modern implementations will be presented. Afterward, some sophisticated examples will be given that showcase the current advances toward the fast, robust, and intuitive identification of noncovalent interactions in real space.

This article is categorized under:

Software > Molecular Modeling

Quantum Computing > Theory Development

Structure and Mechanism > Computational Biochemistry and Biophysics

KEYWORDS

Annotation, Computational biology, Function, Protein, Sequence

1 | INTRODUCTION

Noncovalent interactions (NCIs), both within and between molecules, are important in all branches of chemistry. While individual NCIs are usually weaker than their classically established covalent and ionic counterparts, they boast unmatched ubiquity: they are everywhere, and it is the sum of such many tiny factors that governs, as an emergent

property, complex systems. Just to list a few relevant examples, NCIs are relevant in molecular recognition,¹ protein folding and unfolding,² and the storage of genetic information.^{3,4}

The generalized importance of NCIs, however, signals the gist of the problem. When we speak of NCIs we usually encompass several wildly different physical origins: hydrogen bonds, halogen bonds, π - π stacking, van der Waals interactions, and a long list thereafter. Due to this, chemical intuition which may suffice for covalent bonds often fails to identify NCIs. An undeniable consequence is that the aforementioned list of NCI types is never ending, with newly defined NCI types being added every few years (e.g., π -cation, S-cation, and pnictogen bonds).⁵⁻⁷

At the same time, computationally characterizing NCIs is far from trivial. When approached from the perspective of quantum mechanics, which is holistic, several issues arise immediately. First of all, the tiny energies involved in individual interactions compared with the grand total energy terms from the Hamiltonian. Second, the cooperative nature, which shines in large systems where the exponential scaling of quantum chemical computations can rarely be applied. Luckily, in recent years there has been a significant advancement in computational techniques, both from wavefunction-based approaches⁸ and, perhaps even more so, stemming from density functional theory (DFT).⁹⁻¹¹

Nevertheless, there has to be a link between accurate theory and interpretation. For instance, in the construction of classical many-body potentials or simple representations for machine learning of potential energy surfaces, one does need accurate values for interaction energies but also a physical basis, a fundamental understanding. Many approaches coexist in this regard.¹²⁻¹⁵ Sometimes the basal representation of some NCIs differs wildly between different scientific communities, arising from mathematical models that include significant assumptions (e.g., the multipole expansion) or that only tackle a few types of interaction (e.g., the secondary interaction model¹⁶), with sometimes conflicting results.¹⁷ The underlying issue at hand is the decomposition of interaction energies in several distinct contributions with a chemical interpretation.

Historically, NCIs have been decomposed in several distinct contributions: electrostatics, polarization, exchange, and charge-transfer effects.¹⁸ As a zeroth-order approximation, forces between molecules must arise from the interaction of permanent electric moments over a large distance, due to Coulomb's law. This term is easy to estimate from frozen charge distributions, for example using Symmetry Adapted Perturbation Theory or the Interacting Quantum Atoms framework.^{8,19} However, such interactions will naturally polarize both charge distributions, generating induced electric moments and resulting in higher order couplings that must be truncated at some point. Assuming that exchange and charge-transfer effects are shorter ranged than electrostatics, attractive NCIs are either dominated by polarization terms and thus usually called van der Waals interactions, or mainly electrostatic in nature, which generally results in stronger forces (e.g., hydrogen bonds, π -cation interactions). Unequivocally quantifying exchange and charge-transfer effects is extremely hard.^{20,21}

A possible approach is studying NCIs through the electron density $\rho(\mathbf{r})$ and its derived scalar and vector fields. Such approach shares the key concept of DFT: the electron density can be directly related to the energy, and therefore we should be able to study interactions purely from the density as well. Coincidentally, all contributions to the interaction energy except for zeroth-order electrostatics can be associated with a deformation in $\rho(\mathbf{r})$. These methodologies have several natural interpretative advantages. They are invariant with respect to unitary transformations of molecular orbitals, they are generally robust, and can be examined visually due to their three-dimensional nature. For more than 30 years, such techniques have been used to understand fuzzy chemical concepts, such as bonds and atoms.²²⁻²⁴

Among the real-space framework, the NCI index²⁵ stands as an approach dedicated to NCIs. As we approach the 10th anniversary of the method, which inherits the main advantages of its predecessors (such as Atoms-In-Molecules), an overview of recent implementations, past success and future perspectives is due.

2 | THE NCI INDEX AND ITS INTERPRETATION

2.1 | The reduced density gradient

The NCI index arises from the study of the reduced density gradient, $s(\mathbf{r})$. This gradient was first conceived as a correction for semilocal density approximations in DFT.²⁶ It is a simple function of the electron density, $\rho(\mathbf{r})$, and its gradient (Equation 1):

$$s(\mathbf{r}) = \frac{1}{C_s} \frac{|\nabla\rho(\mathbf{r})|}{\rho(\mathbf{r})^{4/3}}, \quad (1)$$

where $C_s = 2(3\pi^2)^{1/3}$. At first glance, $s(\mathbf{r})$ is an adimensional measurement of the inhomogeneity of the density at a point of space \mathbf{r} , because it measures the ratio at which the density changes with respect to the uniform electron gas. Therefore, it vanishes everywhere in a uniform electron gas. However, it is also a quantity that can be interpreted in real molecular systems, where the electron density is quite far apart from that of an uniform electron gas.

The reduced density gradient does not have an upper bound, and will be maximal when the density vanishes faster than the gradient. This is the case, for example, in the valence density of most systems, but specially when far away from nuclear positions where $\rho(\mathbf{r}) \rightarrow 0$ and consequently $s(\mathbf{r}) \rightarrow \infty$. In general, the situations where it takes very low values are far more interesting, as the lower bound of 0 is well characterized.

There are two types of situations in which $\nabla s(\mathbf{r}) = 0$. The first possibility is that $\nabla\rho(\mathbf{r}) = 0$, and therefore, $\rho(\mathbf{r})$ has a Critical Point (CP). Such points have been thoroughly studied in the context of the AIM theory^{23,27} and thus the points belonging to this situation in $s(\mathbf{r})$ have been termed “AIM-CPs.”²⁸ AIM-CPs are found in most covalent chemical bonds, nuclear positions (cusps), ring centers, and other characteristic emplacements that have already been interpreted by AIM theory, and discussed over the years.²⁹

Likewise, traditionally AIM-CPs are classified according to the components of the Hessian of $\rho(\mathbf{r})$ with respect to $\mathbf{r} = (x, y, z)$ in the CP. Diagonalization of the Hessian $H(\rho, \mathbf{r})$ leads to three eigenvalues λ_1, λ_2 , and λ_3 that add up to the Laplacian of the electron density $\nabla^2\rho(\mathbf{r})$. There are only four possible types of AIM-CPs, depending on $S = \sum_i \lambda_i / |\lambda_i|$, which measures the definiteness of $H(\rho, \mathbf{r})$:

- $S = -3$ for local maxima, generally on nuclear positions.
- $S = -1$ in saddle points which typically appear in covalent bonds (e.g., C–C axis of ethane).
- $S = +1$ in saddle points which typically appear in rings (e.g., center of benzene).
- $S = +3$ for local minima which typically appear in molecular cages (e.g., center of fullerene).

The interpretation of such points is given by the AIM theory. Most typically, they are classified in terms of the Laplacian, $\nabla^2\rho(\mathbf{r})$, into shared-shell (i.e., covalent) interactions if $\nabla^2\rho(\mathbf{r}) < 0$; and closed-shell (e.g., ionic and weak interactions) if $\nabla^2\rho(\mathbf{r}) > 0$. All these situations are recovered by NCI as AIM-CPs.

The other situation in which $\nabla s(\mathbf{r}) = 0$ corresponds to situations in which $\nabla\rho(\mathbf{r}) \neq 0$, which have been called “non-AIM-CPs.” In these points, the following equality holds (Equation 2):

$$\frac{\nabla^2\rho(\mathbf{r})}{\rho(\mathbf{r})} = \frac{4(\nabla\rho(\mathbf{r}))^2}{3\rho^2(\mathbf{r})} \quad (2)$$

From Equation (2) it can be inferred that in this case the Laplacian is always positive, so we are in the closed-shell interactions case. Effectively, these points correspond to regions where the density is varying very slowly, with a global charge depletion.

The situation that such points encompass can be understood from a schematic model of two atoms with a linear combination of exponential Slater type orbital on each. If the atoms are close and the densities overlap, the total density will show the features of a typical covalent AIM-CP. However, if the two orbitals overlap in a region in which their exponential decay is asymptotic ($\nabla\rho(\mathbf{r}) \approx 0$), the resulting density may present a non-AIM-CP (Figure 1).

Such situations are qualitatively identified with local NCIs. Similar observations have been put forward from other contexts: interactions are signaled by deviations from simple exponential decay.^{30,31} Similarly, the annihilation between exponentials of opposite phase is exploited in the Independent Gradient Model, a remarkable derivation from the NCI index methodology.^{32,33}

Due to the continuous nature of $s(\mathbf{r})$, points in which $s(\mathbf{r}) = 0$ are surrounded by low-valued regions. In fact, properties of $s(\mathbf{r})$ isosurfaces are determined by their critical points: components of the surface points originate at minima of the function. Consequently, the analysis is typically performed by using small isosurfaces of $s(\mathbf{r})$, which better reflects the often delocalized nature of NCIs. This methodology is also far less computationally demanding than the calculation of all the CPs of $s(\mathbf{r})$ and allows for a visual merging of spurious local minima.

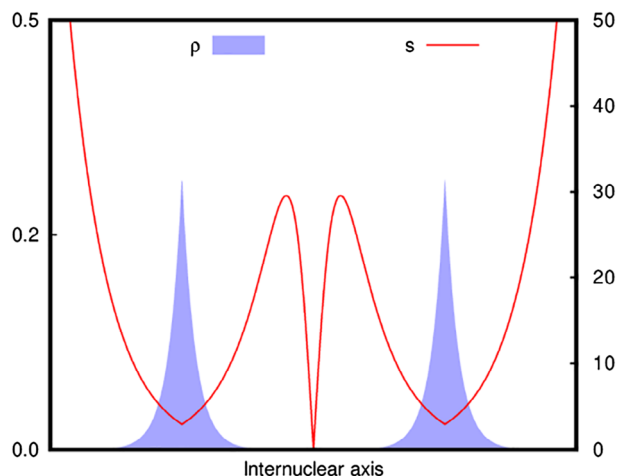


FIGURE 1 ρ and s along the internuclear axis of a model system that is governed by two weakly interacting exponential cusps

2.2 | Physical interpretation

Although an interpretation in terms of exponential decays is understandable from a mathematical standpoint, it lacks connection with physical quantities. $s(\mathbf{r})$ is an indicator of the bosonic character of the system because it is the kernel of the bosonic kinetic energy density $\tau_{\text{bose}}(\mathbf{r})$ (Equations 3 and 4)²⁸.

$$\tau_{\text{bose}}(\mathbf{r}) = \frac{5}{3}s^2(\mathbf{r}) = \frac{\tau_w(\mathbf{r})}{\tau_{\text{TF}}(\mathbf{r})} \quad (3)$$

$$\nabla \tau_{\text{bose}}(\mathbf{r}) = \frac{10}{3}s(\mathbf{r})\nabla s(\mathbf{r}) \quad (4)$$

where $\tau_{\text{TF}}(\mathbf{r}) = 3/10(3\pi^2)^{2/3}\rho(\mathbf{r})^{5/3}$ is the Thomas–Fermi kinetic energy density and $\tau_w(\mathbf{r}) = 1/8(\nabla\rho(\mathbf{r}))^2/\rho(\mathbf{r})$ is the von Weizsäcker kinetic energy density. Recalling that the von Weizsäcker term is appropriate for single-orbital systems, while the Thomas–Fermi term is a typical scaling factor to avoid nuclear preponderance, the physical interpretation of this function is straightforward: $\tau_{\text{bose}}(\mathbf{r})$ measures the single-particle character of the system, which increases whenever $\tau_{\text{bose}}(\mathbf{r}) \rightarrow 0$.

Note that this interpretation is coherent with the previous observations on the behavior of $s(\mathbf{r})$. For instance, nuclear cusps (assuming that the Kato cusp is described through Gaussian functions) will present an AIM-CP, which is a CP of $\rho(\mathbf{r})$ with $S = -3$, and marked single-orbital character. By construction, $\tau_{\text{bose}}(\mathbf{r})$ is not limited to the identification of NCIs. Hence, neither is $s(\mathbf{r})$.

In this sense, using $s(\mathbf{r})$ is based on similar grounds to other real-space functions, as the Electron Localization Function (ELF)^{24,34} the Localized Orbital Locator (LOL),³⁵ and other successful descriptors. In fact, a simple bound function $\chi(\mathbf{r}) = 1/(1 + \tau_{\text{bose}}(\mathbf{r}))$ can be defined that is suitable for the elucidation of bonding patterns. In Figure 2 we can see how the Lewis pattern of CO_2 is revealed by χ and coincides with previous localization functions: nuclear positions, the C–O bond and the lone pairs appear as maxima of χ (minima of τ_{bose}). It should be noted that a structuration appears in the bonding region highlighted by χ which corresponds to an ionic contribution (i.e., a polar covalent bond).³⁶

This is the reason why the NCI index succeeds even when AIM theory fails, and belongs to the significantly more sophisticated descriptors based on the kinetic energy density and/or $H(\rho, \mathbf{r})$. Just like the evolution of DFT has shown, these two quantities often carry useful information. Limiting ourselves to AIM theory, significant chemical features such as lone pairs and weak-interactions would remain invisible. Instead, as shown in Figure 2 these are all simultaneously revealed by NCI.^{37,38}

2.3 | Qualitative analysis

In the previous sections we have detailed why regions with low $s(\mathbf{r})$ correspond with NCIs from both an applied and a theoretical perspective. The simplest way to visual inspect such regions is plotting low-valued isosurfaces, typically s

FIGURE 2 χ , ELF, and LOL along the Z-axis of the CO₂ molecule. Nuclear positions are indicated by the respective atomic symbols

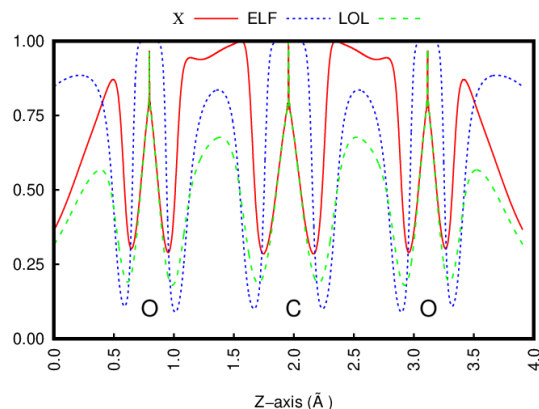


FIGURE 3 $s(\mathbf{r}) = 0.5$ isosurfaces on the acetic acid dimer. (a) with a $\rho(\mathbf{r}) = 0.05$ cutoff (b) with a $\rho(\mathbf{r}) = 0.08$ cutoff (c) without any cutoff

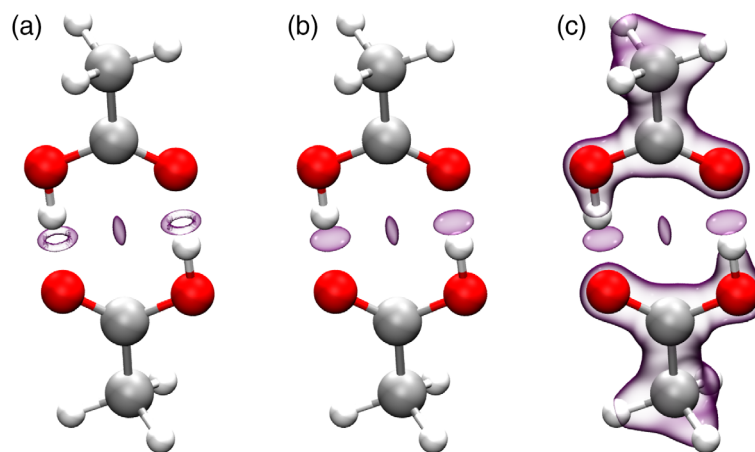
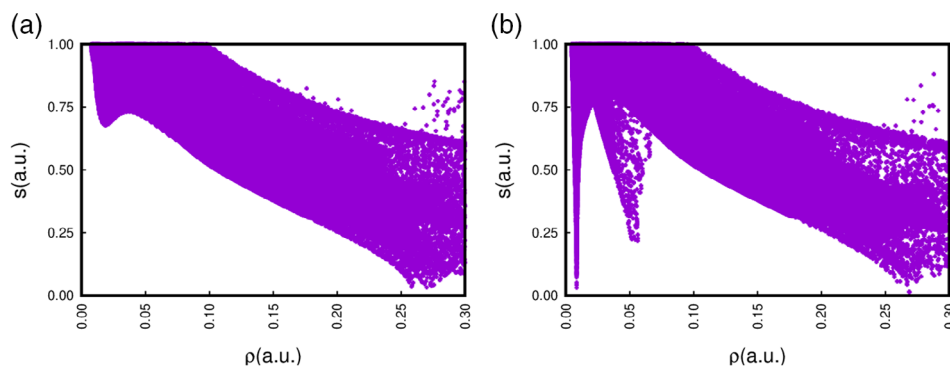


FIGURE 4 $s(\mathbf{r})$ against $\rho(\mathbf{r})$ plots for (a) the acetic acid molecule and (b) the acetic acid dimer as in Figure 3



$(\mathbf{r}) = 0.3\text{--}0.5$, in 3D. However, low $s(\mathbf{r})$ regions also identify all AIM-CPs (e.g., covalent bonds). If one wants to focus on NCI regions only, the simplest approach is to select a small cutoff of $\rho(\mathbf{r})$, because we know that, unlike NCIs, bonds and nuclei have large density values. This is significantly faster and computationally cheaper than characterizing each CP, which would be the more rigorous alternative, and provides a clean view. The effect of this procedure is highlighted in Figure 3, in which all intramolecular covalent interactions are discarded by imposing a simple cutoff.

Establishing a proper cutoff for the density can be done with ease using a 2D representation of $s(\mathbf{r})$ against $\rho(\mathbf{r})$ for all \mathbf{r} . Covalent bonds correspond to the rightmost peak in Figure 4a,b, with higher densities ($\rho(\mathbf{r}) \approx 0.27$). NCIs appear as zeros (or close to zero) only in leftmost region of Figure 4b¹, the dimer, matching chemical insight. The thin peak at $\rho = 0.09$ corresponds to the van der Waals blob in the C–C axis, while the strong hydrogen bonds correspond to the second peak, with $\rho \approx 0.05$. Note that, in this case, an appropriate density cutoff is higher than 0.05 in order to properly accommodate the density of the entire second peak. Therefore, Figure 3a is not an ideal representation, and the strong

hydrogen bonds show a hole that disappears upon increasing the cutoff (as in Figure 3b,c). 2D representations are always advised in order to properly select a density cutoff and avoid this issue.

It is also possible to qualitatively classify interactions to complete the NCI characterization. The previous 2D representations can be unfolded by plotting $s(\mathbf{r})$ against the product of the density and the sign of the second eigenvalue of $H(\rho, \mathbf{r})$. This is normally expressed as $\text{sign}(\lambda_2)\rho(\mathbf{r})$. The sign of λ_2 measures charge accumulation in the perpendicular plane of the interaction. The function $\text{sign}(\lambda_2)\rho(\mathbf{r})$ is able to classify interaction types: strongly attractive (e.g., hydrogen bonds) < 0 , van der Waals $\simeq 0$ (irrespective of the sign) and steric clashes > 0 . For instance, $S = +1$ and $S = +3$ AIM-CPs are revealed as steric clashes from this classification since several atoms are simultaneously contributing to the electron density at these points.

A color code based on $\text{sign}(\lambda_2)\rho$ is often used to connect the 2D and 3D representations. An example is shown in Figure 5 for several base pairs present in RNA. The colored peaks in the 2D graph correspond to the regions with the same colors enclosed by the 3D isosurfaces.

Note that Figure 5b shows the strongest interactions qualitatively, as the peaks belonging to hydrogen bonds are further shifted to the right (more electron density with negative λ_2) and van der Waals interactions are abundant. This is expected because there are two hydrogen bonds and a third, presumably weaker carbon–hydrogen bond thanks to the available oxygen atom in cytosine. This third interaction is absent in Figure 5a and significantly weaker in Figure 5c because there is no proper electronegative atom for the polar hydrogen to interact with. As before, the rightmost peak corresponds to steric clashes in the center of the five-membered rings, which are $S = +1$ AIM-CPs. The position of this peak stays constant in this series because it originates in the hypoxanthine monomer. The hydrogen bonds and van der Waals interactions that constitute the NCI-bound dimer are all captured by the isosurfaces.

Thus, the NCI index is able to effectively reveal and classify NCIs in various systems without any a priori knowledge about them. It is therefore a very powerful tool for identification and interpretation of quantum chemical calculations, but it can also be applied in many more contexts that will be covered in the next sections.

2.4 | Quantitative analysis

Revealing and classifying NCIs is the most important feature of the NCI index method. However, such representations lack any energetic meaning on their own. This is not an irredeemable problem, because the coherent application of the

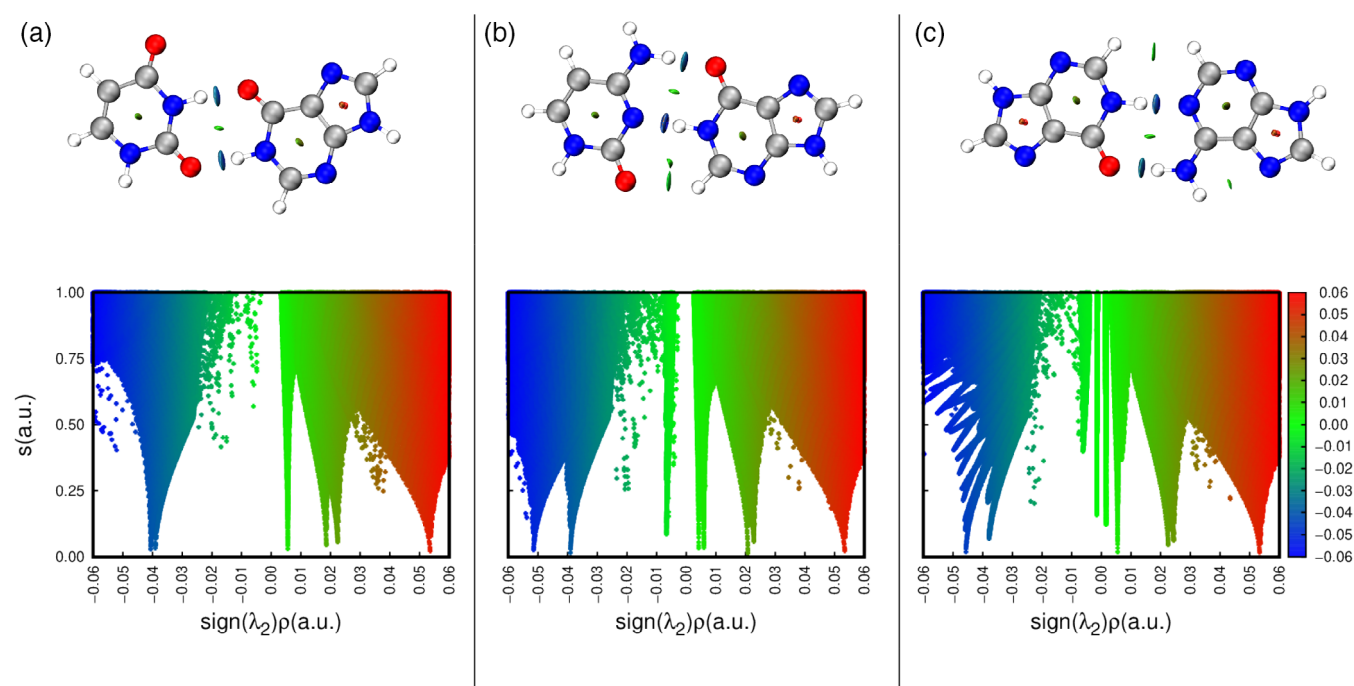


FIGURE 5 $s(\mathbf{r}) = 0.5$ isosurfaces and corresponding 2D plots colored by $\text{sign}(\lambda_2)\rho(\mathbf{r})$ for several dimers in 3D and 2D. (a) Hypoxanthine–adenine, (b) hypoxanthine–cytosine, (c) hypoxanthine–uracil

method stems from DFT. Therefore, from the self-consistent electron density, one can obtain the energy (using a density functional approximation) and also an interpretative picture (using $s(\mathbf{r})$). In any case, it would be desirable to obtain a direct NCI index–interaction energy relationship that quantitatively justifies what is often evident upon visual inspection, which would also enable to go beyond SCF densities (e.g., to obtain energy estimates from promolecular densities).

Remarkably, this would improve upon current methodologies because the interaction energy of individual contacts is generally burdensome and limited to a very small number of atoms.³⁹ Therefore a general and robust measure would provide much needed insight.

As the low density peaks in the 2D diagram can be understood as genuine deformations due to interactions, the key idea is that some subset of points C_{NCI} , or perhaps a bound region Ω_{NCI} given by a NCI surface, S_{NCI} , should account for the interaction locally. This is inspired by, for example, the well-known correlations between $\rho(\mathbf{r})$ in the CP of covalent bonds and their bond dissociation energy, or ELF basin populations which are assimilated to bond orders. However, these approaches lack generality and are applicable only along isoelectronic series.

So far, the most successful, general and robust approach has been obtaining an interacting charge Q_{NCI} by integrating the electron density over a subset of points C_{int} . The most straightforward *Ansatz* is shown in Equation 5.

$$Q_{NCI} = \int_{\mathbf{r} \in C_{NCI}} \rho^n(\mathbf{r}) d\mathbf{r}^3 \quad (5)$$

where $\rho^n(\mathbf{r})$ is the n th power of the density at the points in the C_{NCI} subset. Analogous treatment can be performed using different scalar fields, such as the positive kinetic energy density,^{35,40–44} the molecular virial field^{23,45–47} and the energy density.⁴⁸ However, the most meaningful results are obtained using simple powers of the electron density as the integrand. Another viable option that is native to the NCI index is integrating $\text{sign}(\lambda_2)\rho$, which accounts for the attractive or steric clash nature of the interaction. Typical values of n obtained from fittings lay in the range.^{1,3}

Once an integrand has been chosen, one needs to define C_{NCI} . Several approaches have been tested in this regard as well. In general, it has been found that just using a bounding isovalue of $s(\mathbf{r})$, for instance 0.5, is not enough to properly relate interaction energies with Q_{NCI} . Indeed, this approach enables to characterize bonding but only within the same family.⁴⁹ The question would then be whether very different chemical species can be evenly represented in spite of the fact that some systems are much richer than others in terms of electron density.

The most successful definition so far, based on empirical observations, uses a combination of criteria to define the interacting region. It is based on identifying the points which are intramolecular. This is done as follows: $\rho(\mathbf{r})$ is decomposed in terms of i monomer contributions, $\rho_i(\mathbf{r})$ such as $\rho(\mathbf{r}) = \sum \rho_i(\mathbf{r})$. There are several different ways to do this, including using parametric additive densities (which are trivially separable) and assigning basis functions to fragments according to the center they arise from (i.e., Mulliken or Coulson localization). Any decomposition scheme is viable.

Once the density is partitioned, points in which one of the monomers is dominant are removed using a threshold value γ^{ref} . This first step is meant to remove all intramolecular interaction regions. Then, a maximum value $s^{\text{ref}}(\mathbf{r})$ is used, just like in visualization. The procedure is detailed in Equation (6).

$$\mathbf{r} \in C_{NCI} \begin{cases} s(\mathbf{r}) < s^{\text{ref}}(\mathbf{r}) \\ \rho(\mathbf{r}) < \gamma^{\text{ref}} \rho_i(\mathbf{r}) \forall i \end{cases} \quad (6)$$

γ^{ref} is an empirical threshold value, typically around 0.95 for $i = 1, 2$ dimers. A reasonable isovalue such as $s^{\text{ref}}(\mathbf{r}) = 1.0$ is also recommended. Such a definition provides distinct unconnected regions for individual interactions, which is advantageous.

With this approach, a remarkable correlation ($R^2 \approx .94$) between interaction energies and Q_{NCI} has been obtained in the S66 database.⁵⁰ Additionally, the approach also works with very crude input densities. It has even been shown to enable to dissect dissociation curves into attractive and repulsive contributions.⁵⁰

However, this does not mean that other approaches cannot be meaningful.⁵¹ The correlations observed, which are purely empirical, are strong and robust enough to suggest that, indeed, a transferable *Ansatz* exists that can potentially

be quantitative, just as the visualization procedure seems to work irrespective of the chemical system. Further efforts in this direction are on the way, which may be explored using machine learning approaches as well.⁵²

The open questions in this regard are thus two: what is the proper integrand to consider in Equation (5) and what is the proper definition to consider in Equation (6). A theory-driven answer is on its way. Meanwhile, the approach detailed in Boto et al.⁵⁰ is not far from other approaches in terms of correlation. For instance, the XLYP interaction energies of the S66 set (as collected in the GMTKN55 database⁵³) with respect to the reference data have a value $R^2 = .799$, which improves to $R^2 = .991$ with D3 dispersion corrections. The PBE functional scores $R^2 = .883$ without corrections for the same set. However, the descriptors based on $s(\mathbf{r})$ proposed so far ($R^2 = .94$) do not necessarily require an self-consistent field procedure (see next section for more detail) and have, comparatively, much less empirical parameters.

3 | INPUT DENSITIES

One of the main advantages of the NCI index is the independence from the a priori knowledge of the interaction itself. To calculate $s(\mathbf{r})$ only the electron density is required, so that it can be applied to identify interactions which have not been previously characterized (unlike force fields). In principle, DFT calculations can provide good self-consistent densities, which are not very far away from the exact one, thanks to the Kohn–Sham formulation. Hence, a Kohn–Sham DFT calculation is the most straightforward way to generate an input for an NCI index analysis. In practice, energies in DFT converge with basis set size significantly faster than wavefunction methods, but a triple- ζ quality basis set is recommended for accurate calculations. In this sense, note that a converged energy implies a converged density. For interpretative purposes, DFT-oriented double- ζ basis sets are usually sufficient due to their diffuseness.⁵⁴

However, performing a full self-consistent DFT calculation is not always possible whenever the size of the system is very large, even though linear scaling methods are increasingly developed.⁵⁵ This is unfortunate, as more often than not it is in large systems where NCIs shine the most (e.g., proteins, nucleic acids, and nanomachines). On top of this, these systems also present a large amount of conformational degrees of freedom that further increase the computational cost.

An alternative to linear-scaling DFT is known as partition DFT.⁵⁶ In this approach, the total system is approximated by a series of self-consistent fragment densities, which are then allowed to interact with each other. Analogously, the total density of a large system can be approximated by combining the self-consistent densities of smaller, tractable fragments. By doing so, it is found that regions that correspond to NCIs are often negligibly distorted. This is so because orbital overlap in such regions is near zero.

Therefore, as an approximation, fragment densities which are cheap to calculate can be used to reconstruct a total density, which can be analyzed using $s(\mathbf{r})$. The density cutoff will remove most of the covalent and atomic regions, in which the effect of interfragment interaction would be significantly larger. Thus, at least qualitatively, NCIs can be studied from fragments.

Depending on the desired accuracy, different levels of approximation are available. The full wavefunction is obviously the ideal case (Figure 6a), followed by the sum of localized fragments, which arise from self-consistent monomer wavefunctions that have undergone a localization procedure^{57–59} and later have been orthogonalised. Figure 6b shows the example for NCI derived from a Natural-Bond Orbital localized DFT calculation of each monomer. The simple sum of fragment self-consistent densities is significantly worse than the localization procedure. Figure 6c shows the results for a DFT calculation on each monomer. The cheapest yet crudest approximation is known as the promolecular approximation, in which atomic orbitals are used to reconstruct the full density (Figure 6(d)). Note that levels (c) and (d) formally correspond to densities that arise from wavefunctions that are not properly antisymmetric.

Albeit significantly worse, the promolecular approximation has negligible cost. Atomic densities can be parametrized as exponential functions which have very accurate decaying tails, which are then simply positioned at nuclear positions.^{38,60} The resulting densities and gradients are representative in the weakly interacting areas (Figure 7b), but these densities are usually more diffuse than the calculated counterparts (Figure 7a; figures for other input densities can be found in Supporting Information). Therefore, a lower isovalue of $s(\mathbf{r}) = 0.3$ is usually advised, and higher density values can be expected in such regions. Nevertheless, this is optimal for treating large conformational spaces. The major limitation is accurately treating charged or radical species, which is nigh impossible with such an approach because atomic densities cannot properly reproduce delocalized charge carriers.

FIGURE 6 $s(\mathbf{r}) = 0.5$ isosurfaces colored by $\text{sign}(\lambda_2)\rho(\mathbf{r})$ for the acetic acid dimer with densities from different sources: (a) DFT calculation of the dimer. (b) Natural-Bond Orbital localized DFT calculation of each monomer. (c) DFT calculation on each monomer. (d) $s(\mathbf{r}) = 0.4$ isosurface using atomic densities (promolecular)

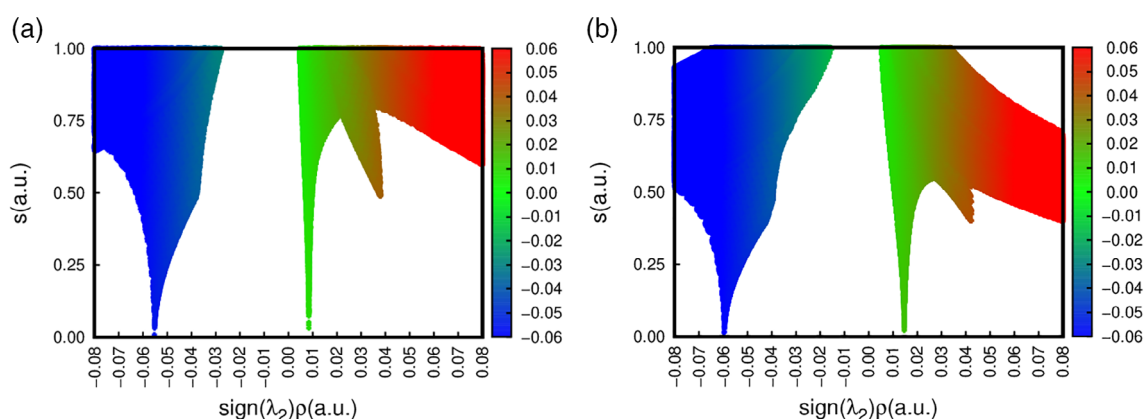
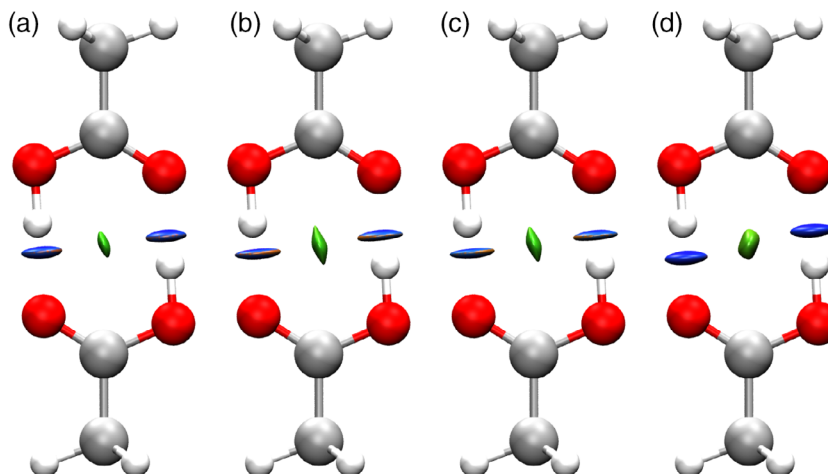


FIGURE 7 2D NCI analysis of the acetic acid dimer using densities from different sources: (a) DFT calculation on the dimer (b) atomic densities (promolecular)

A fifth option is to use experimental densities from X-ray diffraction experiments. This can be done through numerical derivatives of the electron density⁶¹ or after constraining them to a particular wavefunction form.^{62,63} After all, the electron density is an experimentally available observable.

However, it must always be taken into account that mixing densities from different sources is not trivial, and that combining densities from different sources without proper postprocessing might produce very erroneous gradients and hence distorted interpretation. Caution is advised. There is no absolute reason for an interpretation to be good if the density approximation is not.

4 | COMPUTATIONAL IMPLEMENTATION

Several noteworthy remarks have been put forward in the previous sections that contribute toward the scalability and speed of the NCI index analysis. First and foremost, all the points in which $s(\mathbf{r}) = 0$ need not be characterized because a density cutoff is in place that can be inferred from the 2D diagram.

Therefore, grid-based implementations are simple, and just involve calculating $s(\mathbf{r}_j)$ at every point j of a finite grid after checking that $\rho(\mathbf{r}_j)$ is smaller than the density cutoff of choice. The density, which is required in $s(\mathbf{r}_j)$, can be obtained from different sources, as explained in the previous section. For wavefunction based densities, $\nabla\rho(\mathbf{r}_j)$ can be calculated from the derivatives of the basis set functions, which are often analytical. In promolecular densities this is even simpler because of the simple exponential form of atomic densities. The grid is usually set in a way that covers the molecular coordinates, and is denser or coarser depending on the required accuracy. For instance, integrations based

on $s(\mathbf{r})$ will require fine grids to converge. This is due to the presence of higher density points near the boundary of the integration region.

After $s(\mathbf{r}_j)$ is calculated at every point of the grid, values of the reduced density gradient will show regions where single-orbital character is maximal, and thus will reveal NCIs. This algorithm was naively implemented in the first published code for NCI index analysis.⁶⁰

A number of improvements can speed up the procedure significantly. Indeed, the calculation of $s(\mathbf{r}_j)$ is trivially parallelizable if analytical gradients are available. However, the use of dense grids might still be computationally demanding, specially memory-wise. Therefore, an adaptive scheme was proposed recently⁵⁰ to help tackle larger molecules faster and more efficiently.

The adaptive algorithm uses several nested regular grids. The procedure starts with a coarse grid (Figure 8a), computes the required ρ and s in all points of the grid in the active area (violet zone in Figure 8), then builds an α_l -times denser grid containing only the regions of space in which both $s(\mathbf{r}_j) < \alpha_l s_{\text{ref}}$ and $\rho(\mathbf{r}_j) < \alpha_l \rho_{\text{ref}}$. The α_l coefficient is used to make sure peaks are not missed due to the very coarse grid. After the identification of important grid points, ρ and s are computed again, and the process proceeds until the user defined number of steps is reached (Figure 8c). The complete procedure is schematised in Figure 8 for a three-steps implementation in which $\alpha_l = 2$ at each step. Areas without color contain discarded points in which functions are not evaluated anymore. Naturally, the number of iterations and the value of α_l can be adjusted to ensure maximal performance for different steps.

5 | APPLICATIONS OF THE NCI INDEX

The possible applications of the methodology are many and diverse. A few examples will be showcased in this section to illustrate the various fields of application. Most specifically, we will dwell on an example of new bond types (the tetrel bond), material science (adsorption on graphene flakes), and biochemistry (the DNA double strand and a protein–ligand interaction).

5.1 | Analysis of new bonding situations: Tetrel bonds

Analogous to hydrogen bonds, tetrel bonds are NCI where the bridging atom between a Lewis base and an electron withdrawing atom is one of the tetrel (C, Si, Ge, etc.) family, which presents a local electron deficiency (σ -hole).⁶⁴ In a way, they are analogous to pnictogen and chalcogen bonds, but the relevance of carbon in organic chemistry and biochemistry makes tetrel bonds more enticing. For instance, the significance of tetrel bonds as a preliminary step of SN2 reactions has been pointed out.⁶⁵

At the same time, carbon is electronegative and small, therefore the σ -hole of substituted alkyl moieties are small and tetrel bonds with such holes are generally weak and consequently hard to model. Furthermore, they might bypass chemical intuition, and thus be ignored whenever they play a key role. Even weak NCIs might be determining in transition structures. The NCI index, which needs no a priori knowledge of the underlying interactions, can be used to reveal tetrel bonds—and any other weak interaction.

Six different models were optimized at the CAM-B3LYP-D3BJ/def2-TZVP level: F–CH₃··B and F–SiH₃··B with B=H₂O, NH₃, CH₂O. Very flat minima were found in all cases corresponding to interactions between the available electron pairs in B and the σ -hole of the tetrel moiety. NCI index analysis for all six systems is shown in Figure 9 in 3D.

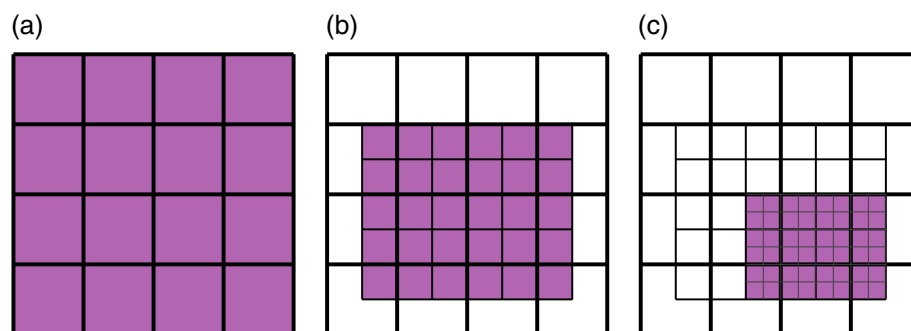


FIGURE 8 Schematic representation of a three-step adaptive grid procedure with $\alpha_l = 2$. Active regions are colored purple, colorless areas are inactive

As it can be seen in Figure 9a–c, the tetrel bond imposes a linear arrangement of B with respect to the C–F axis. Equilibrium distances are significantly longer than those present in covalent bonds, and the interaction is identified as weak by the NCI index criteria due to the low density in the region. However, treading down the group, Si is far less electronegative than C. In Figure 9d–f a much thicker, bluish isosurface can be seen, signaling increased interaction strength. In fact, both Figure 9d,e are comparable to a typical NCI index depiction of a hydrogen bond due to the increased basicity of ammonia and water compared to formaldehyde.

This is in agreement with the equilibrium distances, which are reduced significantly for Si compared to C: 3.00, 3.18, and 3.01 Å in Figure 9a–c, respectively shrink to 2.72, 2.56, and 2.90 Å in Figure 9d–f. However, distances do not capture the behavior of the system: counterpoise corrected interaction energies increase at a much different rate, just from 1.74 kcal/mol in Figure 9c to 2.96 kcal/mol in Figure 9f, but much more significantly in the other cases: 1.91 kcal/mol Figure 9a to 4.45 kcal/mol Figure 9d for H₂O and 2.10 kcal/mol in Figure 9b to 8.40 kcal/mol in Figure 9e for NH₃. Simply inspecting the NCI analysis using $s(\mathbf{r})$ may have sufficed to guess that, in spite of the similar distances and the involvement of an oxygen atom, the interaction energy in H₂O···SiH₃F (Figure 9d) is larger than in CH₂O···SiH₃F (Figure 9f).

All in all, being based on the electron density, the NCI index can be useful to identify unexpected NCIs, including the newest additions, such as is the case of tetrel bonds.

5.2 | Analysis of heterogeneous catalysis: Graphene sites

Graphene is a promising carbon allotrope with many applications in development. A plausible use of graphene layers is the enhanced adsorption of chemically inert species such as CO₂. However, the chemical and physical properties of graphene can also be tuned with the inclusion of boron and nitrogen atoms in the periodic lattice.^{66,67}

While calculating adsorption pathways of small molecules in graphene is feasible with modern DFT methods, interpreting results is not always straightforward. Why is a site preferred over another? As an example, B3LYP-D3BJ/def2-TZVP calculations were performed of the CO₂ molecule adsorbed over different graphene flakes, including B and N-doped cases. Local minima were found in the potential energy surface, and the resulting densities were analyzed using the NCI index. 3D results are presented in Figure 10.

Visualizing the NCI index results, it becomes apparent that sites are determined by balancing out local pairwise interactions between atoms. For instance, in the case of boron doping (Figure 10a), two O···B interactions can be seen, oxygen atoms sitting just atop boron atoms, which suggest a deficit of electron density in the B-substituted sites that makes them suitable for nucleophilic attack. A different result is observed for the nitrogen doped case (Figure 10b), where oxygen atoms sit on top of the middle of the triply substituted triazine ring, revealing a O- π hole interaction. It is interesting to note that O···N interactions seem to arise in spite of the total positive charge of the flake. This points to a plausible perpendicularly adsorbed conformation, with one terminal O atom in the middle of the ring.

Finally, in Figure 10a non local interactions arise, and the location of the minima seems to be fundamentally arising from the van der Waals interaction between the π -system of the flake and the charge distribution of the CO₂ molecule.

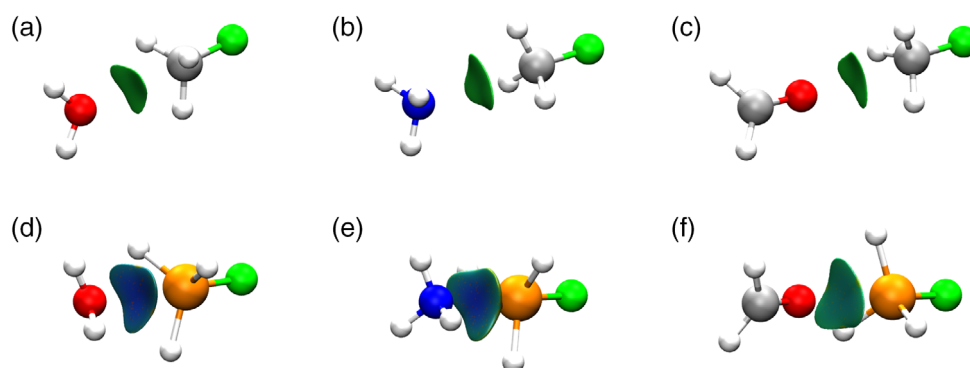


FIGURE 9 $s(\mathbf{r}) = 0.5$ isosurfaces colored by $sign(\lambda_2)\rho(\mathbf{r})$ for several tetrel bonds: (a) F–CH₃···OH₂ (b) F–CH₃···NH₃ (c) F–CH₃···OCH₂ (d) F–SiH₃···OH₂ (e) F–SiH₃···NH₃ (f) F–SiH₃···OCH₂. C, H, Si, F, N, and O atoms are colored gray, white, orange, green, blue, and red, respectively

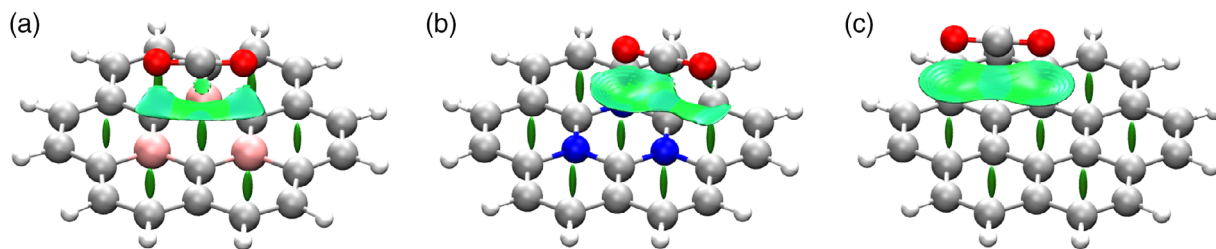


FIGURE 10 CO₂ adsorption on top of different graphene-like flakes: (a) B-doped graphene, (b) N-doped graphene flake, (c) nonsubstituted graphene flake

Therefore, just by computationally sampling some conformations and using the NCI index, we can rationalize that adsorption on nonsubstituted graphene will not be as effective for the capture and/or activation of CO₂ as in the substituted analogues. Furthermore, we can suggest that the adsorption mechanisms will differ between B-doped graphene, which favors a planar conformation with strong O···B interactions, and N-doped graphene which presents an interaction between oxygen atoms and the π -hole of the triazine moiety.

5.3 | Analysis of interactions in biomolecules along a molecular dynamics simulation

The acceleration of NCIPlot 4.0 over the previous versions of the code opens new possibilities in the world of biomolecular applications at the dynamical level. Indeed, molecular dynamics simulations can be used to study large biomolecular systems in realistic conditions over significant timescales. However, such simulations generate very abundant data that requires a significant effort to analyze. Additionally, NMR in solution is becoming the method of choice for the experimental determination of protein structures, as they are able to account for their inherent flexibility. Using the simplest promolecular approximation, multiple frames exploring the conformations of a single system can be studied using the NCI index at a negligible cost. The interested reader is directed to Reference 68, which details the guidelines for the application of NCI integrals to the biomolecular field.

In order to understand interstrand interactions in nucleic acids, each of the strands can be defined as a fragment. Along with the `intermolecular` keyword, this simple procedure effectively removes intra-strand interactions and isolates interstrand π -stacking and hydrogen bonding (Figure 11).

In an MD simulation of the system at equilibrium, we expect interstrand interactions to be converged. In order to be able to evaluate the strength of all interstrand hydrogen bonds and π -stacking with a single descriptor, we can follow the evolution of the strongly attractive ($\text{sign}(\lambda_2)\rho$ between -0.1 and -0.02) and weakly attractive ($\text{sign}(\lambda_2)\rho$ between -0.02 and 0.02) NCI integrals along the molecular dynamics trajectories. Results, shown in Figure 12, indicate that both contact types are essentially constant along the simulation, which can be therefore considered converged with respect to interstrand NCIs.

This approach is particularly advantageous when a collective description of a number of hydrogen bonds is required. Indeed, most classical dynamics force fields do not have an explicit term to account for hydrogen bonds, which are described by the electrostatic and van der Waals ones. For this reason, analysis of the hydrogen bond network is generally performed after the dynamics with a separate module using geometric criteria (distances and angles between hydrogen bond donors and acceptors). This kind of analysis is therefore capable of following the distribution and frequency of individual hydrogen bonds, but not of evaluating directly their collective strength. NCI integrals, conversely, provide a compact descriptor for all contacts belonging to a predefined density range.

In Figure 12, for instance, it can also be observed how, in the beginning of the trajectory, a small decrease in interstrand hydrogen bonds is counteracted by an improved interstrand π -stacking. Therefore, range integration is a tool for the analysis and interpretation of MD calculations that requires no a priori definition of NCIs whatsoever.

This kind of analysis is not only useful to interpret MD trajectories, but also to assess their convergence. Let us consider the example of a protein–ligand interaction, a model of amyloid- β (1–40) (A β 40) fibril in complex with two fluorescent markers, Thioflavin-T and NIAD4 (Figure 13).⁶⁹

Our starting point is the classical molecular dynamics simulations of the Thioflavin-T/A β 40 and NIAD-4/A β 40 complexes. From the trajectories, one hundred frames were extracted for each complex, stripped of water

FIGURE 11 $s(\mathbf{r}) = 0.3$ isosurface in an intramolecular calculation fo a DNA fragment

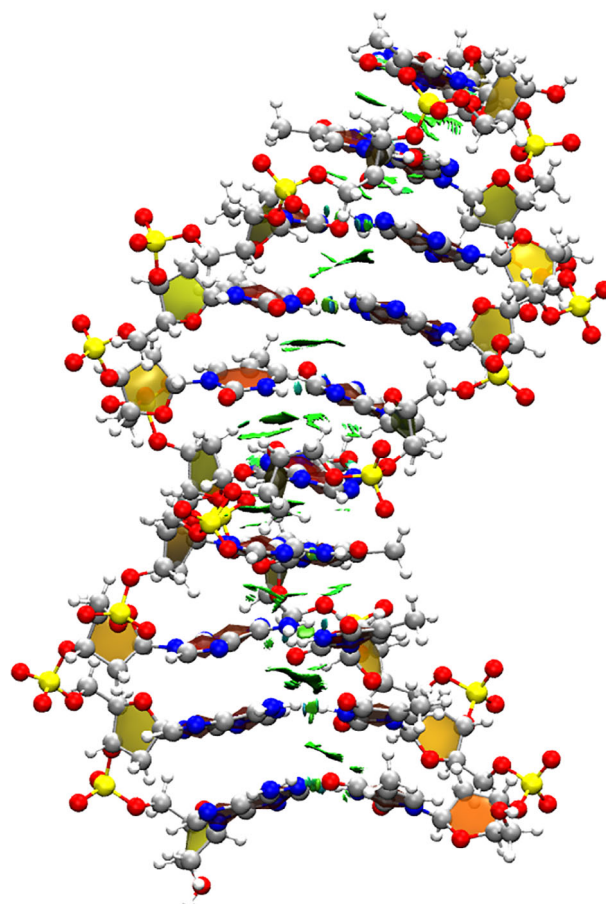
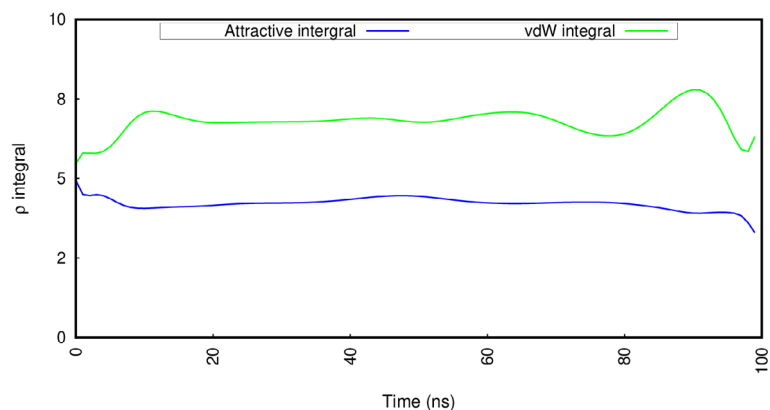


FIGURE 12 Integrals over time for different sign $(\lambda_2)\rho$ intervals. Integration was performed with $\gamma^{ref} = 0.95$ and $s^{ref}(\mathbf{r}) = 1.0$



molecules and ions, and processed with NCIPLLOT 4.0. A promolecular run was performed on each frame in the LIGAND mode, setting the cutoffs on the density and reduced density gradient at 0.2 and 1.0, respectively, and using 0.1 Å increments. A cutoff of 4 Å was used for intermolecular interactions.

The resulting 2D plots along the dynamics trajectories are presented in Supporting Information, and show how the protein–ligand contacts evolve along the frames of the dynamics, with the formation and disruption of hydrogen bonds that contribute to the stabilization of the complexes.

For a more quantitative view of the network of steric clashes and attractive contacts, it is possible to plot the value of the $\int \text{sign}(\lambda_2)\rho^2$ integral along the frames of the dynamics simulations integrating over three ranges: $\text{sign}(\lambda_2)\rho$: -0.05 to -0.01 , corresponding to attractive interaction, -0.01 to 0.01 to van der Waals, and 0.01 – 0.05 to the so-called steric clashes. The plots for Thioflavin-T and NIAD-4 are reported in Figures 14 and 15, respectively, and show that there is a

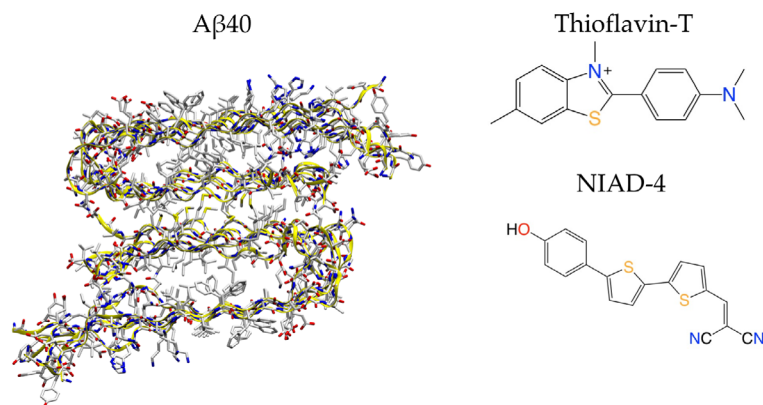


FIGURE 13 Structure of an amyloid- β (1–40) fibril, PDB code 2LMN, and of Thioflavin-T and NIAD-4, fluorescent markers for amyloid detection

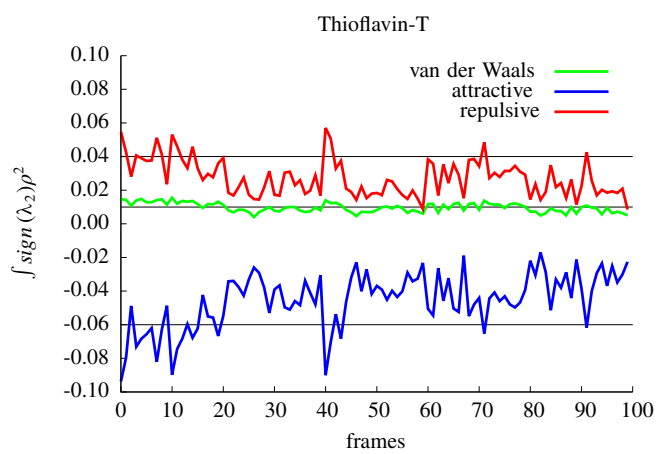


FIGURE 14 Evolution of $\int \text{sign}(\lambda_2)\rho^2$ along the 100 dynamics frames of Thioflavin-T/A β 40 integrated over three ranges of $\text{sign}(\lambda_2)\rho$: -0.05 to -0.01 (attractive), -0.01 to 0.01 (van der Waals), 0.01 to 0.05 (repulsive). Black lines are guides to the eyes

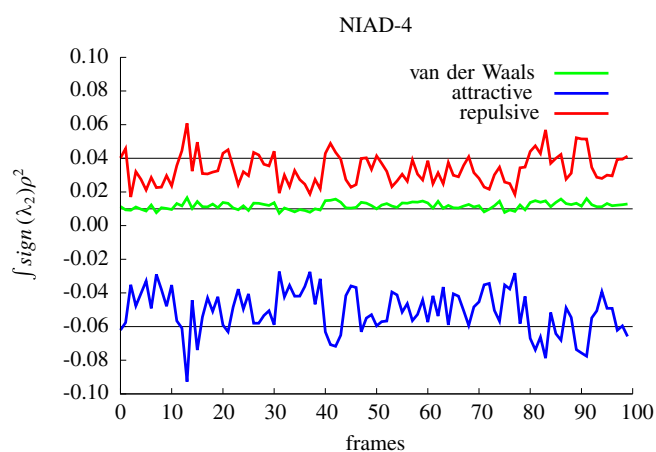


FIGURE 15 Evolution of $\int \text{sign}(\lambda_2)\rho^2$ along the 100 dynamics frames of NIAD-4/A β 40 integrated over three ranges of $\text{sign}(\lambda_2)\rho$: -0.05 to -0.01 (attractive), -0.01 to 0.01 (van der Waals), 0.01 to 0.05 (repulsive). Black lines are guides to the eyes

significant difference between the two molecules. While for NIAD-4 (Figure 15) the integrals corresponding to the three types of interaction are constant along the dynamics (oscillating approximately around 0.03 for steric clashes, 0.01 for van der Waals and -0.06 for attraction), indicating that our dynamics is equilibrated with respect to ligand-protein contacts, for Thioflavin-T we can appreciate a global change of the pattern of noncovalent interaction. Indeed, the integrals of both steric clashes and the attractive component decrease along the frames, indicating that the system is not equilibrated but is adjusting its binding pose. The interesting point here is that this difference can hardly be appreciated looking at the bare interaction energy along the frames, because the simultaneous loss of attractive contacts and steric clashes leads to contributions of opposite sign to the interaction energy that can cancel out or at least partially compensate each other.⁵² This means that small differences in the interaction energy can correspond to large changes in the network of noncovalent interactions.

This analysis can be used to complete and unravel the values of binding energies; in the widespread MM/PBSA methodology, for instance, the binding energy is evaluated as an average result on a set snapshots extracted from a molecular dynamics trajectory. Performing this NCIPLOT analysis on the same snapshots is a quick way to tell whether the network of weak interactions that are accounted for by the binding energy are constant or subject to fluctuations, which in turn is informative on the reliability of the binding energy evaluation.

6 | CONCLUSIONS AND OUTLOOK

The NCI index has been successfully used for the identification, characterization and analysis of NCIs for about 10 years now. We have reviewed the physical basis of the method, the nuanced details of its interpretation, and some key technical features and advances. The existence—and the role—of the density-based cutoff is particularly important to notice in order to properly analyze results.

Furthermore, we have introduced the latest developments in NCI index analysis. In terms of quantitative analysis, the most relevant *Ansatz* has been presented, which has been shown to correlate with interaction energies over a significant chemical space. In any case, we have shown how the empirical correlations that are known can be exploited to analyze NCIs in several contexts. Attention from a wider scientific community is brought upon the two highlighted questions: what would be a sensible *Ansatz* that is not simply based on $\rho(\mathbf{r})$? and, coupled to it, what is the ideal definition of the interacting region? Further efforts will be devoted to these two questions in the near future.

NCI calculations can be coupled with localization techniques to partition the system of interest. This is particularly viable because NCIs are usually studied between closed-shell systems. Therefore, the exponential scaling on DFT calculations can be minimized and very large systems can be analyzed using very accurate densities. Coupled to the newest algorithmic developments, gigantic biomolecular structures can be tackled, originating from either experimental crystallography or molecular dynamics simulations. Indeed, NCI provides in a compact format the fundamental information on the evolution of contacts in biosystems as a function of time. It allows to look at the individual regions of *sign* (λ_2) ρ corresponding to attractive, van der Waals contacts and steric clashes rather than at the global interaction energy for each frame. This information can be used both to analyze MD results as well as to assess their equilibration.

All in all, the NCI index offers a fast, intuitive understanding of the interactions that take place in the system, which will hopefully give it another 10 years of helping people characterize weak interactions.

ACKNOWLEDGMENTS

All authors express their gratefulness to LabEx CALSIMLAB (public grant ANR-11-LABX-0037-01 constituting a part of the “Investissements d’Avenir” program—reference: ANR-11-IDEX-0004-02). This work has received funding from the European Research Council (ERC) under the European Union’s Horizon 2020 research and innovation programme (grant agreement No 810367), project EMC2 (Jean-Philip Piquemal and Yvon Maday). Alessandra Carbone, Jean-Philip Piquemal, and Yvon Maday acknowledge the funding of the Institut Universitaire de France. Rubén Laplaza thanks ED 388 for a PhD grant. Yvon Maday and Chaoyu Quan acknowledge the funding from the PICS-CNRS and the PHC PROCOPE 2017 (Project No. 37855ZK).

CONFLICT OF INTEREST

The authors have declared no conflicts of interest for this article.

AUTHOR CONTRIBUTIONS

Ruben Laplaza: Data curation; formal analysis; investigation; validation; visualization; writing-original draft. **Francesca Peccati:** Data curation; formal analysis; investigation; validation; visualization. **Roberto A. Boto:** Methodology; software; writing-review and editing. **Chaoyu Quan:** Methodology; software. **Alessandra Carbone:** Funding acquisition; writing-review and editing. **Jean Phillippe piquemal:** Funding acquisition; supervision. **Yvon Maday:** Methodology; supervision. **Julia Contreras:** Conceptualization; formal analysis; funding acquisition; methodology; resources; software; supervision; writing-review and editing.

ORCID

Julia Contreras-García  <https://orcid.org/0000-0002-8947-9526>

ENDNOTE

¹ A deviation might have been spotted even in the case of the monomer. This is indeed a weak O–H intramolecular interaction.

RELATED WIREs ARTICLES

[An overview of the Amber biomolecular simulation package](#)
[Quantum-mechanical condensed matter simulations with CRYSTAL](#)
[Noncovalent interactions in biochemistry](#)

REFERENCES

1. Persch E, Dumele O, Diederich F. Molecular recognition in chemical and biological systems. *Angew Chem Int Ed*. 2015;54:3290–3327.
2. Ben-Naim A. The role of hydrogen bonds in protein folding and protein association. *J Phys Chem*. 1991;95:1437–1444.
3. Watson JD, Crick FHC. Molecular structure of nucleic acids: A structure for deoxyribose nucleic acid. *Nature*. 1953;171:737–738.
4. Mignon P. Influence of the interaction on the hydrogen bonding capacity of stacked DNA/RNA bases. *Nucleic Acids Res*. 2005;33:1779–1789.
5. Ma JC, Dougherty DA. The cation– π interaction. *Chem Rev*. 1997;97:1303–1324.
6. Motherwell WB, Moreno RB, Pavlakos I, et al. Noncovalent interactions of π systems with sulfur: The atomic chameleon of molecular recognition. *Angew Chem Int Ed*. 2017;57:1193–1198.
7. Brammer L. Halogen bonding, chalcogen bonding, pnictogen bonding, tetrel bonding: Origins, current status and discussion. *Faraday Discuss*. 2017;203:485–507.
8. Hohenstein EG, Sherrill CD. Wavefunction methods for noncovalent interactions. *Wiley Int Rev: Comp Mol Sci*. 2011;2:304–326.
9. Burns LA, Vázquez-Mayagoitia Á, Sumpter BG, Sherrill CD. Density-functional approaches to noncovalent interactions: A comparison of dispersion corrections (DFT-D), exchange-hole dipole moment (XDM) theory, and specialized functionals. *J Chem Phys*. 2011;134:084107.
10. Grimme S, Hansen A, Brandenburg JG, Bannwarth C. Dispersion-corrected mean-field electronic structure methods. *Chem Rev*. 2016;116:5105–5154.
11. Stöhr M, Voorhis TV, Tkatchenko A. Theory and practice of modeling van der Waals interactions in electronic-structure calculations. *Chem Soc Rev*. 2019;48:4118–4154.
12. Hermann J, Alfè D, Tkatchenko A. Nanoscale π – π stacked molecules are bound by collective charge fluctuations. *Nat Commun*. 2017;8:14052.
13. van der Lubbe SCC, Zaccaria F, Sun X, Guerra CF. Secondary electrostatic interaction model revised: Prediction comes mainly from measuring charge accumulation in hydrogen-bonded monomers. *J Am Chem Soc*. 2019;141:4878–4885.
14. Pollice R, Chen P. A universal quantitative descriptor of the dispersion interaction potential. *Angew Chem Int Ed*. 2019;58:9758–9769.
15. Meyer B, Barthel S, Mace A, et al. DORI reveals the influence of noncovalent interactions on covalent bonding patterns in molecular crystals under pressure. *J Phys Chem Lett*. 2019;10:1482–1488.
16. Jorgensen WL, Pranata J. Importance of secondary interactions in triply hydrogen bonded complexes: Guanine-cytosine vs uracil-2,6-diaminopyridine. *J Am Chem Soc*. 1990;112:2008–2010.
17. Popelier PLA, Joubert L. The elusive atomic rationale for DNA Base pair stability. *J Am Chem Soc*. 2002;124:8725–8729.
18. Kitaura K, Morokuma K. A new energy decomposition scheme for molecular interactions within the Hartree-Fock approximation. *Int J Quant Chem*. 1976;10:325–340.
19. Blanco MA, Martín Pendás A, Francisco E. Interacting quantum atoms: A correlated energy decomposition scheme based on the quantum theory of atoms in molecules. *J Chem Theory Comp*. 2005;1:1096–1109.
20. Misquitta AJ. Charge transfer from regularized symmetry-adapted perturbation theory. *J Chem Theory Comp*. 2013;9:5313–5326.
21. Deng S, Wang Q, Ren P. Estimating and modeling charge transfer from the SAPT induction energy. *J Comput Chem*. 2017;38:2222–2231.
22. Bader RF. *Atoms in molecules*. Oxford, UK: Oxford University Press, 1990.
23. Bader RF. A bond path: A universal indicator of bonded interactions. *Chem A Eur J*. 1998;102:7314–7323.
24. Becke AD, Edgecombe KE. A simple measure of electron localization in atomic and molecular systems. *J Chem Phys*. 1990;92:5397–5403.
25. Johnson ER, Keinan S, Mori-Sanchez P, Contreras-Garcia J, Cohen AJ, Yang W. Revealing noncovalent interactions. *J Am Chem Soc*. 2010;132:6498–6506.
26. Perdew JP, Burke K, Ernzerhof M. Generalized gradient approximation made simple. *Phys Rev Lett*. 1996;77:3865–3868.
27. Bader RFW, Tang TH, Tal Y, Biegler-Koenig FW. Molecular structure and its change: Hydrocarbons. *J Am Chem Soc*. 1982;104:940–945.
28. Boto RA, Contreras-García J, Tierny J, Piquemal J-P. Interpretation of the reduced density gradient. *Mol Phys*. 2016;114:1406–1414.
29. Shahbazian S. Why bond critical points are not “bond” critical points. *Chem A Eur J*. 2018;24:5401–5405.
30. de Silva P, Korchowiec J, Wesolowski TA. Atomic shell structure from the single-exponential decay detector. *J Chem Phys*. 2014;140:164301.

31. de Silva P, Corminboeuf C. Simultaneous visualization of covalent and noncovalent interactions using regions of density overlap. *J Chem Theory Comp.* 2014;10:3745–3756.
32. Lefebvre C, Rubez G, Khartabil H, Boisson J-C, Contreras-García J, Hénon E. Accurately extracting the signature of intermolecular interactions present in the NCI plot of the reduced density gradient versus electron density. *Phys Chem Chem Phys.* 2017;19:17928–17936.
33. Lefebvre C, Khartabil H, Boisson J-C, Contreras-García J, Piquemal J-P, Hénon E. Independent Gradient Model: a new approach for probing strong and weak interactions in molecules from wave function calculations. *ChemPhysChem.* 2017;19:724–735.
34. Savin A, Nesper R, Wengert S, Fässler TF. ELF: The electron localization function. *Angew Chem Int.* 1997;36:1808–1832.
35. Schmider H, Becke A. Chemical content of the kinetic energy density. *J Mol Struct (THEOCHEM).* 2000;527:51–61.
36. Boto RA, Piquemal J-P, Contreras-García J. Revealing strong interactions with the reduced density gradient: A benchmark for covalent, ionic and charge-shift bonds. *Theor Chem Acc.* 2017;136:139.
37. Lane JR, Contreras-García J, Piquemal J-P, Miller BJ, Kjaergaard HG. Are bond critical points really critical for hydrogen bonding? *J Chem Theory Comput.* 2013;9(9):3263–3266.
38. Contreras-García J, Boto RA, Izquierdo-Ruiz F, Reva I, Woller T, Alonso M. A benchmark for the non-covalent interaction (NCI) index or is it really all in the geometry? *Theo. Chem Acc.* 2016;135:242.
39. Pendás AM, Blanco MA, Francisco E. Two-electron integrations in the quantum theory of atoms in molecules. *J Chem Phys.* 2004;120:4581–4592.
40. Becke A. Hartree-Fock exchange energy of an inhomogeneous electron gas. *Int J Quant Chem.* 1983;23:1915–1922.
41. Cohen L. Local kinetic energy in quantum mechanics. *J Chem Phys.* 1979;70:788–789.
42. Cohen L. Representable local kinetic energy. *J Chem Phys.* 1984;80:4277–4279.
43. Abramov YA. On the possibility of kinetic energy density evaluation from the experimental electron-density distribution. *Acta Crystall Sect A: Found Crystall.* 1997;53:264–272.
44. Finzel K. ELF and its relatives—a detailed study about the robustness of the atomic shell structure in real space. *Int J Quant Chem.* 2014;114:1546–1558.
45. Keith T, Bader R, Aray Y. Structural homeomorphism between the electron density and the virial field. *Int J Quant Chem.* 1996;57:183–198.
46. Pendás AM. Stress, virial, and pressure in the theory of atoms in molecules. *J Chem Phys.* 2002;117:965–979.
47. Pendás AM, Francisco E, Bueno AG, Vela JG, Costales A. Emergent scalar and vector fields in quantum chemical topology. *Applications of topological methods in molecular chemistry.* Cham, Switzerland: Springer, 2016; p. 131–150.
48. Cremer D, Kraka E. A description of the chemical bond in terms of local properties of electron density and energy. *Croatica Chemica Acta.* 1984;57:1259–1281.
49. Saleh G, Gatti C, Presti LL. Energetics of non-covalent interactions from electron and energy density distributions. *Computational and Theoretical Chemistry.* 2015;1053:53–59.
50. Boto R, Peccati F, Laplaza R, et al. NCIPLLOT4: fast, robust and quantitative analysis of noncovalent interactions. *J Chem Theo Comp.* 2020;16:4150–4158.
51. Contreras-García J, Johnson ER, Yang W. Analysis of hydrogen-bond interaction potentials from the electron density: Integration of noncovalent interaction regions. *J Phys Chem A.* 2011;115:12983–12990.
52. Peccati F, Desmedt E, Contreras-García J. Regression approach to accurate interaction energies using topological descriptors. *Comput Theor Chem.* 2019;1159:23–26.
53. Goerigk L, Hansen A, Bauer C, Ehrlich S, Najibi A, Grimme S. A look at the density functional theory zoo with the advanced GMTKN55 database for general main group thermochemistry, kinetics and noncovalent interactions. *Phys Chem Chem Phys.* 2017;19:32184–32215.
54. Zheng J, Xu X, Truhlar DG. Minimally augmented Karlsruhe basis sets. *Theor Chem Acc.* 2010;128:295–305.
55. Nakata A, Futamura Y, Sakurai T, Bowler DR, Miyazaki T. Efficient calculation of electronic structure using O(N) density functional theory. *J Chem Theory Comp.* 2017;13:4146–4153.
56. Elliott P, Burke K, Cohen MH, Wasserman A. Partition density-functional theory. *Phys Rev A.* 2010;82:024501.
57. Carpenter JE, Weinhold F. Transferability of natural bond orbitals. *J Am Chem Soc.* 1988;110:368–372.
58. Meyer B, Guillot B, Ruiz-Lopez MF, Jelsch C, Genoni A. Libraries of extremely localized molecular orbitals. 2. Comparison with the Pseudoatoms transferability. *J Chem Theory Comp.* 2016;12:1068–1081.
59. Meyer B, Guillot B, Ruiz-Lopez MF, Genoni A. Libraries of extremely localized molecular orbitals. 1. Model molecules approximation and molecular orbitals transferability. *J Chem Theory Comput.* 2016;12:1052–1067.
60. Contreras-García J, Johnson ER, Keinan S, et al. NCIPLLOT: A program for plotting noncovalent interaction regions. *J Chem Theory Comp.* 2011;7:625–632.
61. Saleh G, Gatti C, Lo Presti L, Contreras-García J. Revealing non-covalent interactions in molecular crystals through their experimental electron densities. *Chem A Eur J.* 2012;18:15523–15536.
62. Jayatilaka D, Grimwood DJ. Tonto: A Fortran based object-oriented system for quantum chemistry and crystallography. *Computational Science — ICCS 2003.* Berlin, Heidelberg: Springer, 2003; p. 142–151.
63. Arias-Olivares D, Wieduwilt EK, Contreras-García J, Genoni A. NCI-ELMO: A new method to quickly and accurately detect noncovalent interactions in biosystems. *J Chem Theory Comp.* 2019;15:6456–6470.
64. Bauzá A, Mooibroek TJ, Frontera A. Tetrel bonding interactions. *The Chemical Record.* 2016;16:473–487.

65. Grabowski S. Tetrel bond– σ -hole bond as a preliminary stage of the SN2 reaction. *J Phys Chem Chem Phys*. 2014;16:1824–1834.
66. Pan F, Li B, Deng W, et al. Promoting electrocatalytic CO2 reduction on nitrogen-doped carbon with sulfur addition. *Appl Catal Environ*. 2019;252:240–249.
67. Sreekanth N, Nazrulla MA, Vineesh TV, Sailaja K, Phani KL. Metal-free boron-doped graphene for selective electroreduction of carbon dioxide to formic acid/formate. *Chem Commun*. 2015;51:16061–16064.
68. Peccati F. NCILOT4 guide for biomolecules: An analysis tool for noncovalent interactions. *J Chem Inf Model*. 2020;60:6–10.
69. Peccati F, Pantaleone S, Riffet V, et al. Binding of Thioflavin T and related probes to polymorphic models of amyloid- β fibrils. *J Phys Chem B*. 2017;121:8926–8934.

SUPPORTING INFORMATION

Additional supporting information may be found online in the Supporting Information section at the end of this article.

How to cite this article: Laplaza R, Peccati F, A. Boto R, et al. NCILOT and the analysis of noncovalent interactions using the reduced density gradient. *WIREs Comput Mol Sci*. 2021;11:e1497. <https://doi.org/10.1002/wcms.1497>